https://dx.doi.org/10.22161/ijaers.711.34 ISSN: 2349-6495(P) | 2456-1908(O)

Study on the effect of nitrogen content and cooling rate on the ferrite number of austenitic stainless steels

André de Albuquerque Vicente[1,3], Peter Aloysius D'silva[1], Sibi Sadanandan[1], Tiago Felipe de Abreu Santos[2], Jorge Alberto Soares Tenório[3]

[1]ESAB Middle East & Africa,Plot No. S20134, Jebel Ali Free Zone (South), PO Box 8964, Dubai, United Arab Emirates;
[2]Department of Mechanical Engineering, Universidade Federal de Pernambuco, Av. da Arquitetura, s/n, Cidade Universitária, Recife, PE, Brazil;
[3]Department of Chemical Engineering, Universidade de São Paulo, Rua do Lago,250, Cidade Universitária, São Paulo, SP, Brazil.

Received: 18 Sept 2020; Received in revised form: 7 Nov 2020; Accepted: 18 Nov 2020; Available online: 29 Nov 2020

Abstract**—** *In order to better understanding the effect of nitrogen content in shielding gases and different cooling rates on the volume fraction of δ ferrite in welded deposits through GTAW, the microstructures of four welded joints of austenitic stainless steel, were studied. The deposits were produced using the same welding electrode ER 316L2.4 mm and welding parameters, but different shielding gases from pure argon to mixture with N_2, and different cooling rates. One pair of the welding deposits was produced with 100% Ar and the other one with 98% Ar+2% N_2. The weld pads produced with the same shielding gas were submitted to different cooling rates, being cooled in air and water. The chemical compositions and the variation of the volume fractions of δ ferrite in the deposits were measured. It was observed pickup of nitrogen and, consequently, decreasing of the volume fraction of δ ferrite in the all weld metals produced with 98% Ar+2% N_2as the shielding gas. The weld pads cooled in water presented less δ ferrite when compared to those produced using the same shielding gas but cooled in air. The results confirm that nitrogen is a strong austenite stabilizer and that higher cooling rates reduce the δ ferrite volume fraction in austenitic stainless steels. Complementary techniques of microstructural analysis were used, such as optical emission spectrometry, optical microscopy and quantitative image analysis.*
Keywords**— Austenitic stainless steels; Cooling rate; Ferrite number; Nitrogen; Solidification mode.**

I. INTRODUCTION

In welding of high alloy steels, the δ ferrite content is normally estimated from the constitution diagrams such as the Schaeffler**[1]**, DeLong **[2]** and Kotechi**[3]**.

In these diagrams, the δ ferrite contents of various welds had been measured experimentally by either metallography (Schaeffler) or magnetic methods (DeLong and WRC–92).**[4]**

Table 1 shows the expressions of chromium and nickel equivalents proposed by Schaeffler **[1]**, DeLong **[2]** and Kotechi**[3]**.

Table 1 -Cr_{eq} and Ni_{eq} formulae used for estimating the delta-ferrite content from constitution diagrams[4-7]

Constitution Diagram	
Schaeffler Diagram (1949)	Cr_{eq} = Cr + Mo + 1.5xSi + 0.5xNb
	Ni_{eq} = Ni + 30xC + 0.5xMn
DeLong Diagram (1973)	Cr_{eq} = Cr + Mo + 1.5xSi + 0.5xNb
	Ni_{eq} = Ni + 30xC + 30xN + 0.5xMn
WRC-92 Diagram (1992)	Cr_{eq} = Cr + Mo + 0.7xNb
	Ni_{eq} = Ni + 35xC + 20xN + 0.25xCu

https://dx.doi.org/10.22161/ijaers.711.34 *ISSN: 2349-6495(P) | 2456-1908(O)*

Most of the compositions of commercial stainless steels, are in the iron-rich side of the ternary Fe-Cr-Ni equilibrium diagram, between 50 and 70% of iron in weight. The initial solidifying phase is determined by the position of the alloy with respect to the liquidus surface, which under equilibrium conditions proceeds toward the eutectic and peritectic transformations, before solidification is complete. Figure 1 shows the pseudo-binary equilibrium diagram on the vertical section of Fe–Cr–Ni equilibrium diagram at a constant Fe content of 70% in weight. It is commonly used to identify the primary solidifying phases or solidification modes for various compositions of different stainless steels. **[4-17]**

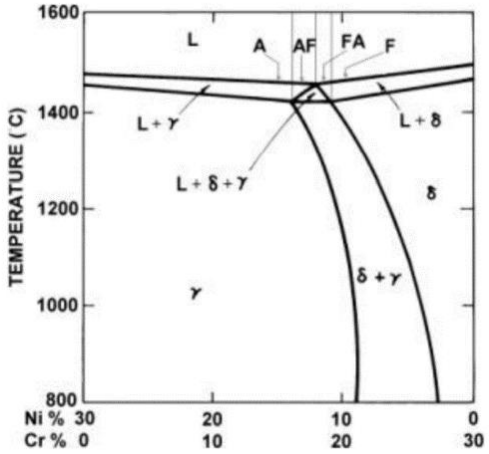

Fig.1: Pseudo-binary section of the Fe–Cr–Niternary diagram at 70% Fe, showing solidification modes; A - fully austenitic, AF - austenitic–ferritic, FA - ferritic–austenitic and F - fully ferritic.[8, 15]

According to Suutala's work**[18-22]**, the Cr_{eq}/Ni_{eq} ratio is fundamental in determining the solidification mode of austenitic stainless steels.

Considering the cooling rates ranges applicable in welding, when the Cr_{eq}/Ni_{eq} ratio < 1.5, the solidification may be austenitic (mode I) or austenitic-ferritic (mode II). When the ratio 1.5 <Cr_{eq}/Ni_{eq}< 2.0 the solidification will be ferritic-austenitic (mode III). And finally, when Cr_{eq}/Ni_{eq} ratio > 2.0 the solidification will be ferritic (mode IV). **[5-14, 18-22]**

The cooling rate is of fundamental importance for the microstructure resulting from the solidification of austenitic stainless steels.

Figure 2 shows the changes in the Schaeffler diagram proposed by Johnson, Grabaek, Johansen, Sarholt Kristensen and Wood **[23],** that shows an increase in the austenitic field for ultra-high cooling rates.

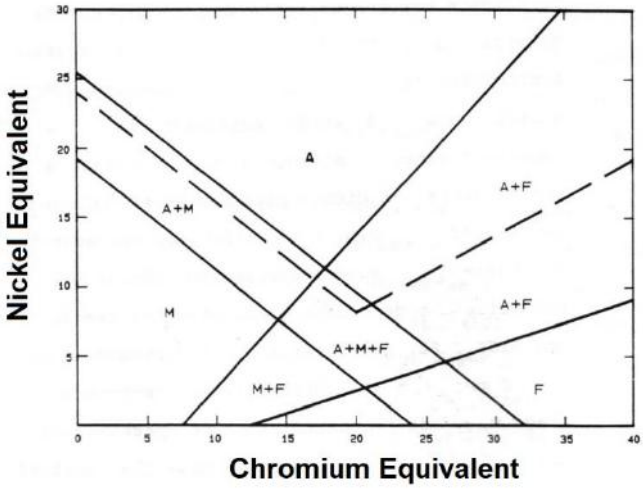

Fig.2: Modified Schaeffler diagrams for cooling rates of around 10^6 K/s.[5, 23]

O. Hammar and U. Svensson**[24]** showed that the addition of carbon and nitrogen decreases the volumetric fraction of ferrite in austenitic stainless steels.Taking as an example the austenitic stainless steel of type AISI 316, which usually solidifies through a ferritic-austenitic solidification mode. With the increasing of carbon and nitrogen contents as alloying elements, the solidification mode changes to austenitic-ferritic. There is, therefore, acarbon equivalent value that can change how this steel solidifies.

Ceq =% C + 0.65% N **(Equation 1)**

Figure 3 shows the change in the solidification mode of stainless steel of type AISI 316 as a function of carbon equivalent.

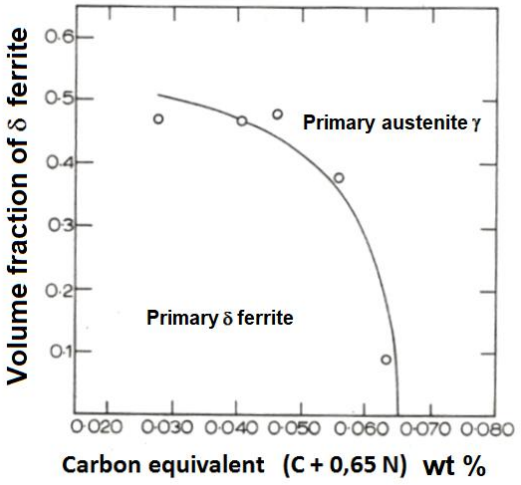

Fig.3: Change in the solidification mode of stainless steel of type AISI 316 as a function ofC_{eq}. [5,6,24]

https://dx.doi.org/10.22161/ijaers.711.34 *ISSN: 2349-6495(P) | 2456-1908(O)*

II. EXPERIMENTAL

Four welded joints of austenitic stainless steel produced using GTAW process with different shielding gases and different cooling rates were studied. The deposits were produced using the same welding electrode ER 316L 2.4 mm according to AWS 5.9 from the same heat. One pair of the welding deposits was produced with 100% Ar, and the other one with 98% Ar+2% N_2 as shielding gases. The weld pads produced with the same shielding gas were submitted to different cooling rates, being one cooled to100 °C in air and other one in water just after each welding bead. The GTAW welding machine was adjusted to allow a stable welding. All the weld pads were produced with the same travel speeds to have similar heat inputs for all the four samples. In order to minimize the effect of base metal chemical composition, 6 layers of 5 beads each were deposited. Overlapping passes were used, depositing approximately 25 mm on the base metal that was an AISI 304L type stainless steel. The weld pads were cut in longitudinal and transversal directions. Chemical analyzes were carried out in all samples at 20 mm from the base metal, by means of an optical emission spectrometer, according to ASTM E 1086-08. **[25]**

Transversal and longitudinal samples were embedded in hot-cure resin (bakelite). The conventional manual polishing was applied using water sandpapers (100, 240, 320, 400, 600 and 1000 mesh) in order to standardize the surface finish of the samples. A cloth polishing with 9, 3 and 1 μm diamond abrasive paste was carried out in this sequence. The samples were electrolytically attacked in 20% NaOH solution, 6V, for 90 seconds. This allowed the microstructural characterization of the samples through optical microscopy. The quantitative metallographic analysis for the determination of volumetric fractions of δ ferrite and austenite were performed according to ASTM E 562 ed. 08, **[26]** using a 4X5 grid (20 points) with a magnification of 400X in 30 different regions per test piece.

III. RESULTS AND DISCUSSION

Table 2 presents the welding parameters used to weld the samples. It is important to emphasize that the deposits were produced using the welding electrode ER 316L 2.4 mm according to AWS 5.9 from the same heat, and similar welding parameters, but different shielding gases and different cooling rates. One pair of the welding deposits was produced with 100% Ar, and the other one with 98% Ar+2% N_2asshielding gases.The weld pads produced with the same shielding gas were submitted to different cooling rates, being one cooled to 100 °C in air and other one in water just after each welding bead.

Table 2–Welding parameters.

Welding wire (ER316L 2.4 mm)	Shielding gas	Flow (l/min)	Current (A)	Tension (V)	Travel Speed (mm/min)	Heat Input (kJ/mm)
Sample 1 (air)	Ar	18	215	19	185	1,32
Sample 2 (air)	98%Ar + 2%N_2	18	210	19	180	1,33
Sample 3 (water)	Ar	18	215	19	190	1,29
Sample 4 (water)	98%Ar + 2%N_2	18	210	19	185	1,29

Table 3 presents the chemical compositions and the calculations of C_{eq}, according to O. Hammar and U. Svensson**[24],** of four deposits.

The calculations of C_{eq} were done using **Equation 1**.

Table 3– Chemical compositions and the calculations of C_{eq},

	C	Si	Mn	P	S	Cr	Ni	Mo	Cu	N	Ceq
ER316L (FM)	0,010	0,40	1,76	0,025	0,011	18,91	12,33	2,55	0,26	0,028	0,028
Sample 1 (Ar - air)	0,008	0,33	1,73	0,025	0,011	18,60	12,20	2,51	0,25	0,042	0,035
Sample 2 (Ar+N_2 - air)	0,008	0,36	1,75	0,025	0,011	18,62	12,18	2,53	0,25	0,140	0,099

https://dx.doi.org/10.22161/ijaers.711.34 *ISSN: 2349-6495(P) | 2456-1908(O)*

Sample 3 (Ar - water)	0,008	0,35	1,72	0,025	0,011	18,63	12,22	2,53	0,25	0,043	0,036
Sample 4 (Ar+N_2 - water)	0,008	0,37	1,76	0,025	0,011	18,71	12,17	2,55	0,25	0,140	0,099

The results presented on table 3, show that the welded joints produced through GTAW present the least change in the chemical composition when compared to the filler wire, with the exception on the concentration of nitrogen.
Figure 4 shows the concentrations of nitrogen (% by weight) of the filler metal ER 316L and all weld metals.

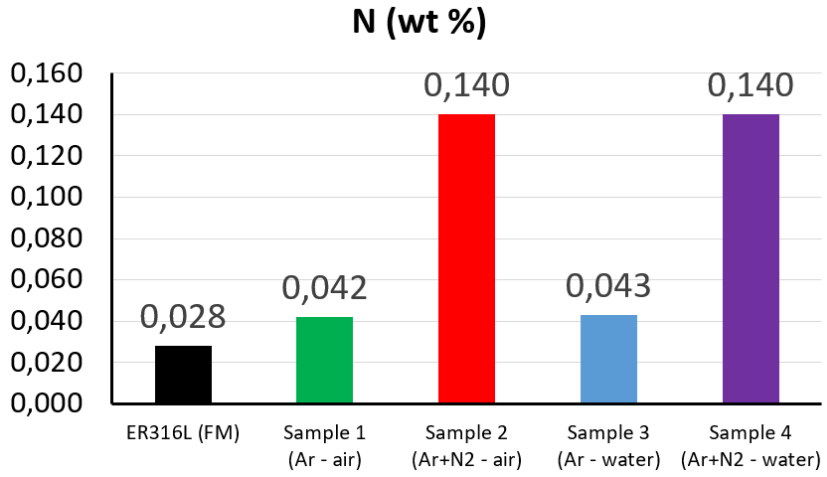

Fig.4: Concentrations of N (% by weight) of the filler metal ER 316L and all weld metals.

There is some loss of carbon, silicon, manganese, chromium and nickel. It is observed pick up of nitrogen for all the four weld pads when compared to the nitrogen content of the filler metal, from 150% when the shielding gas is pure argon, to 500% in the case of 98% Ar + 2% N_2.

Figure 5 shows the concentrations of C, Si, Mn Cr, Ni and Mo (% by weight) of the filler metal ER 316L and all weld metals.

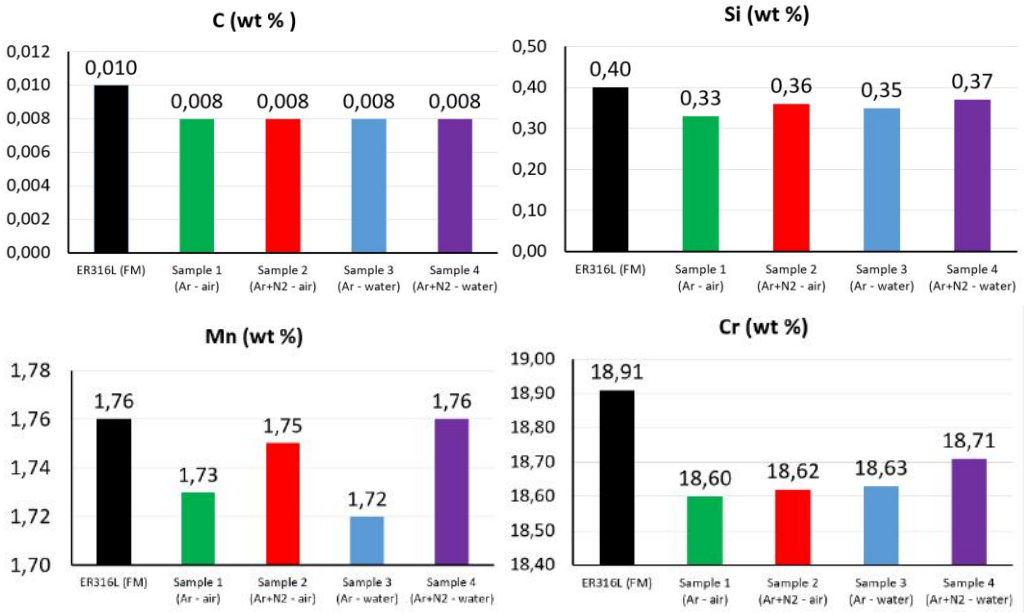

https://dx.doi.org/10.22161/ijaers.711.34 *ISSN: 2349-6495(P) | 2456-1908(O)*

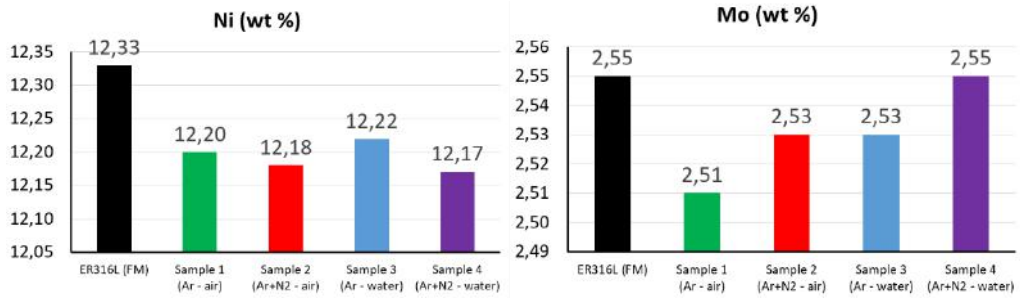

Fig.5: Concentrations of C, Si, Mn, Cr, Ni and Mo (% by weight) of the filler metal ER 316L and all weld metals.

Table 4 presents calculated values ofCr_{eq},Ni_{eq} and Cr_{eq}/Ni_{eq} ratio according to the expressions of chromium and nickel equivalent staken from Table 1.

Table 4– Cr_{eq}, Ni_{eq} and Cr_{eq}/Ni_{eq} ratio according to the expressions of chromium and nickel equivalents proposed by Schaeffler, De Long and Kotechi.

	Schaeffler Diagram (1949)			**DeLong Diagram (1973)**			**WRC-92 Diagram (1992)**		
	Cr_{eq}	**Ni_{eq}**	**Cr_{eq}/Ni_{eq}**	**Cr_{eq}**	**Ni_{eq}**	**Cr_{eq}/Ni_{eq}**	**Cr_{eq}**	**Ni_{eq}**	**Cr_{eq}/Ni_{eq}**
ER316L (FM)	22,06	13,51	**1,63**	22,06	14,35	**1,54**	21,46	13,31	**1,61**
Sample 1 (Ar - air)	21,61	13,31	**1,62**	21,61	14,57	**1,48**	21,11	13,38	**1,58**
Sample 2 (Ar+N_2 - air)	21,69	13,30	**1,63**	21,69	17,50	**1,24**	21,15	15,32	**1,38**
Sample 3 (Ar - water)	21,69	13,32	**1,63**	21,69	14,61	**1,48**	21,16	13,42	**1,58**
Sample 4 (Ar+N_2 - water)	21,82	13,29	**1,64**	21,82	17,49	**1,25**	21,26	15,31	**1,39**

Figure 6 shows the variations of the Cr_{eq} and Ni_{eq} values (% by weight) of the filler metal ER 316L and all weld metals.

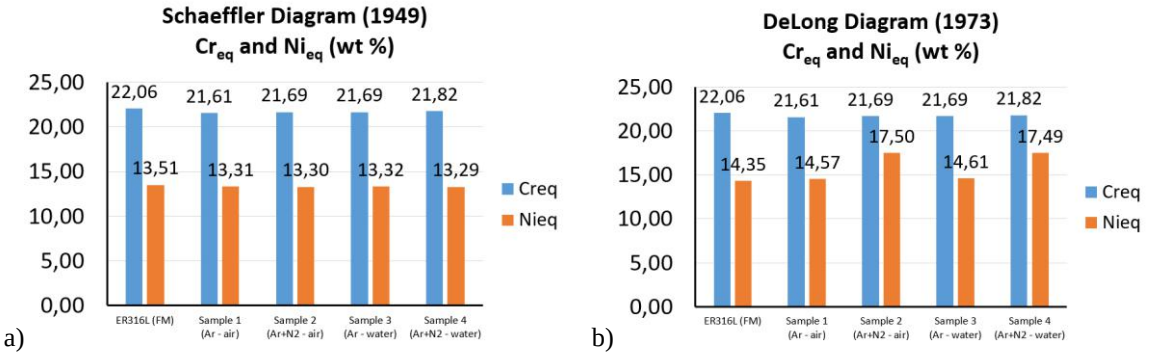

https://dx.doi.org/10.22161/ijaers.711.34 *ISSN: 2349-6495(P) | 2456-1908(O)*

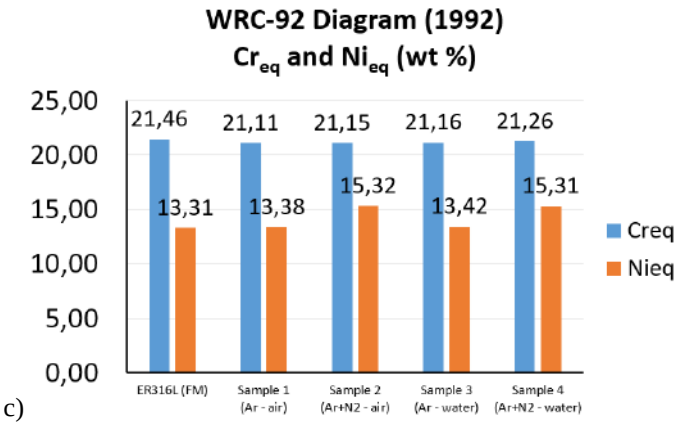

c)

Fig.6: Cr_{eq} and Ni_{eq} values (% by weight) of the filler metal ER 316L and all weld metals, according to the expressions of chromium and nickel equivalents proposed by:
a) Schaeffler, b) DeLongand c) Kotechi.

Figure 7 shows the variations of the Cr_{eq}/Ni_{eq} ratio of the filler metal ER 316L and all weld metals.

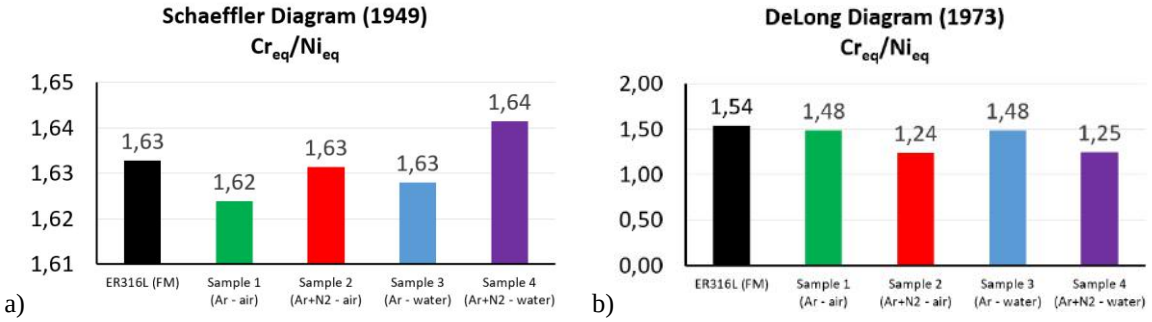

a)

b)

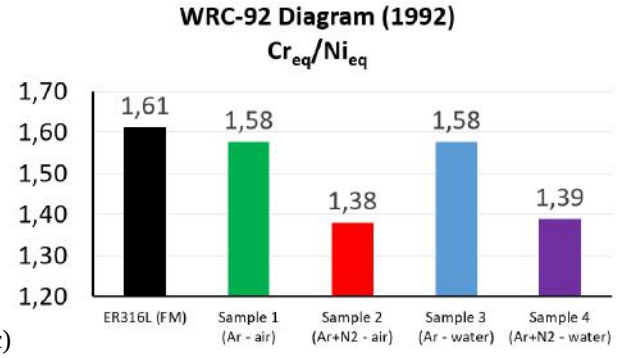

c)

Fig.7: Cr_{eq}/Ni_{eq} ratio of the filler metal ER 316L and all weld metals, according to the expressions of chromium and nickel equivalents proposed by:a) Schaeffler, b) DeLongand c) Kotechi.

Table 5 presents the volume fractions of δ ferrite measured through metallographic analysis in 30 different regions per test piece.

Table 5– Volume fractions of δ ferrite measured through optical microscopy.

Volume fraction of δ ferrite	Mean	95%CI	%RA
Sample 1(Ar - air)- Transversal	8.5	1.8	11.8
Sample 1(Ar - air)-Longitudinal	4.6	2.0	8.4

https://dx.doi.org/10.22161/ijaers.711.34 *ISSN: 2349-6495(P) | 2456-1908(O)*

Sample 1(Ar - air)- Average	**7.7**	**1.6**	**9.2**
Sample 2(Ar+N_2 - air) - Transversal	1.0	1.4	8.2
Sample 2(Ar+N_2 - air) - Longitudinal	0.3	1.2	7.1
Sample 2(Ar+N_2 - air) - Average	**0.5**	**1.3**	**7.4**
Sample 3(Ar - water) - Transversal	8.0	1.7	10.2
Sample 3(Ar - water) - Longitudinal	4.2	1.5	8.1
Sample 3(Ar - water) - Average	**6.8**	**1.8**	**8.7**
Sample 4(Ar+N_2 - water) - Transversal	0.3	1.5	8.6
Sample 4(Ar+N_2 - water) - Longitudinal	0.1	1.0	8.4
Sample 4(Ar+N_2 - water) - Average	**0.2**	**1.5**	**9.0**

The volumetric fractions of δ ferrite verified in the longitudinal direction are smaller than those verified for the transversal direction in the four welded specimens.

As discussed earlier, the results confirm that the nitrogen is a strong austenite former. The samples welded through GTAW using 98% Ar + 2% N_2as shielding gas, sample 2 and sample 4, presented lower volume fraction of δ ferrite.

The increasing in cooling rate results in reduction of the volume fraction of δ ferrite.

The sample welded through GTAW using 98% Ar + 2% N_2as shielding gas and cooled in water, sample 4, presented the lower volume fraction of δ ferrite.

IV. CONCLUSIONS

Nitrogen is a strong austenite former.

The shielding gas is of paramount importance on the ferrite number of the jointswelded through GTAW.The welded joints produced using 98% Ar + 2% N_2as shielding gas, presented lower volume fraction of δ ferrite.

The variations of Cr_{eq} and Ni_{eq}, and the Cr_{eq}/Ni_{eq} ratio of the welded joints suggest that welded joints produced using 98% Ar + 2% N_2as shielding gas, solidified through the austenitic-ferritic (mode II).

The increasing in cooling rate results in reduction of the volume fraction of δ ferrite.

REFERENCES

[1] SCHAEFFLER, A. L.. **Constitution diagram for stainless steel weld metal**. Metal Progress, vol. 56, n.5, p. 680-680B, 1949.

[2] DeLONG, W. T.. **A modified phase diagram for stainless steel weld metals.**Metal Progress, p. 98-100B, 1960.

[3] D.J. KOTECHI; D. T. A. SIEWERT. **WRC – 92 Constitution Diagram for Stainless Steel Weld Metals: a Modification of the WRC – 1988 Diagram**. Welding Journal 71 (5), 171–178, 1992.

[4] M. Vasudevan, M. Murugananth, A.K. Bhaduri, **Application of Bayesian neural network for modeling and prediction of FN in austenitic stainless steel welds**, in: H. Cerjak, H.K.D.H. Bhadeshia (Eds.), Mathematical Modelling of Weld Phenomena—VI, Institute of Materials, 2002, pp. 1079–1099.

[5] Vicente, A. A.. **Estudo da resistência à oxidação ao ar a altas temperaturas de um aço inoxidável austenítico microligado ao cério soldado pelo processo mig/mag com diferentes gases de proteção.** Tese de Doutorado, Escola Politécnica, Universidade de São Paulo, São Paulo. 2017. https://doi:10.11606/T.3.2017.tde-05092017-103140.

[6] VICENTE, A. A.; D'SILVA, P. A.; JOS, B.; SANTOS, T. F. A.; TENÓRIO, J. A. S..**Study on the effect of ferrite number on impact toughness of austenitic stainless steels at low temperatures.** International Journal of Advanced Engineering Research and Science, 7(10), pp.102-111, 2020. https://doi.org/10.22161/ijaers.710.11

[7] VICENTE, A. A.; D'SILVA, P. A.; SANTOS, I. L.; AGUIAR, R. R.; JUNIOR, A. B. B;SANTOS, T. F. A..**The effect of shielding gases in the Ferrite Number of austenitic stainless steels joints through GMAW.** International Journal of Advanced Engineering Research and Science, 7(7), pp.332-341, 2020. https://doi.org/10.22161/ijaers.77.37.

[8] VICENTE, A. A.; D'SILVA, P. A.; SOUZA, R. L.; SANTOS, I. L.; AGUIAR, R. R.; JUNIOR, A. B. B..**The use of duplex stainless steel filler metals to avoid hot cracking in GTAW welding of austenitic stainless steel AISI 316L.** International Journal of Advanced Engineering Research and Science, 7(6), pp.345-355, 2020. https://doi.org/10.22161/ijaers.76.43.

[9] VICENTE, A. A.; SOUZA, R. L.; ESPINOSA, D. C. R.; AGUIAR, R. R.; PAUL, P.. **Effect of relative plate thickness in the heat flow and cooling rate during welding of super duplex stainless steel.** Saudi Journal of Engineering and Technology, 5 (5), 244-150. Scholars

Middle East Publishers, Dubai, United Arab Emirates, 2020. https://doi.org/10.36348/sjet.2020.v05i05.005.

[10] VICENTE, A. A.; SANTOS, I. L.; JUNIOR, A. B. B.; ESPINOSA, D. C. R.; TENÓRIO, J. A. S.. **Study of the Distribution of Cr, Mo, Ni and N in δ Ferrite and Austenite in Duplex Stainless Steels**. Saudi Journal of Engineering and Technology, 5 (4), 156-162. Scholars Middle East Publishers, Dubai, United Arab Emirates, 2020. https://doi.org/10.36348/sjet.2020.v05i04.005.

[11] Santa-Cruz, L. A., Machado, G., Vicente, A. A. et al. **Effect of high anodic polarization on the passive layer properties of superduplex stainless steel friction stir welds at different chloride electrolyte pH values and temperatures.**Int J Miner Metall Mater 26, 710–721 (2019). https://doi.org/10.1007/s12613-019-1790-0.

[12] Marques, I. J., Vicente, A. D. A., Tenório, J. A. S., & Santos, T. F. D. A. (2017). **Double kinetics of intermetallic phase precipitation in UNS S32205 duplex stainless steels submitted to isothermal heat treatment**. Materials Research, 20, 152-158.https://doi.org/10.1590/1980-5373-mr-2016-1060.

[13] A. de Albuquerque Vicente, J.R.S. Moreno, D.C.R. Espinosa, T.F. de Abreu Santos, J.A.S. Tenório. **Study of the high temperature oxidation and Kirkendall porosity in dissimilar welding joints between FE-CR-AL alloy and stainless steel AISI 310 after isothermal heat treatment at 1150 °C in air.**J. Mater. Res. Technol. 8(2), 1636 (2019). https://doi.org/10.1016/j.jmrt.2018.11.009.

[14] Vicente, A. A.; Cabral, D. A.; Espinosa, D. C. R.; Tenório, J. A. S.. **Efeito dos gases de proteção na microestrutura e nas cinéticas de oxidação a altas temperaturas ao ar de juntas soldadas de um aço inoxidável austenítico através do processo MIG/MAG.** Tecnol. Metal. Mater. Min., vol.14, n4, p.357-365, 2017. https://doi.org/10.4322/2176-1523.1264.

[15] Shankar, V.; Gill, T.P.S.; Mannan, S.L. et al. **Solidification cracking in austenitic stainless steel welds.** Sadhana 28, 359–382 (2003). https://doi.org/10.1007/BF02706438

[16] MARQUES, Igor Jordão; SILVA, Flavio J.; SANTOS, Tiago Felipe de Abreu. **Rapid precipitation of intermetallic phases during isothermal treatment of duplex stainless steel joints produced by friction stir welding.** Journal of Alloys and Compounds, Volume 820, 2020. https://doi.org/10.1016/j.jallcom.2019.153170.

[17] Santa Cruz, L. A., Marques, I. J., Urtiga Filho, S .L. et al. **Corrosion Evaluation of Duplex and Superduplex Stainless Steel Friction Stir Welds Using Potentiodynamic Measurements and Immersion Tests in Chloride Environments.** Metallogr. Microstruct. Anal. 8, 32–44 (2019). https://doi.org/10.1007/s13632-018-0506-6.

[18] SUUTALA, N.; **TAKALO**, T.; MOISIO, T.. **Ferritic-Austenitic Solidification mode in Austenitic Stainless Welds.**Metalurgical Transactions A, vol 11A, p. 717-725, 1980.

[19] SUUTALA, N.; MOISIO, T.. **Use of chromium and nickel equivalents in considering solidification mode in austenitic stainless steel welds.**Solidification and Casting Metals, London, The Metals Society, p. 310- 314, 1979.

[20] SUUTALA, N.; TAKALO, T.; MOISIO, T.. **The relationship between solidification and microstructure in austenitic-ferritic stainless steel welds.**Metallurgical Transactions A, vol. 10A, p.512-514, 1979.

[21] TAKALO, T.; SUUTALA, N.; et al.. **Austenitic solidification mode in austenitic stainless steel welds.**Metallurgical Transactions A, vol. 10A, p. 1173-1181, 1979.

[22] SUUTALA, N.; TAKALO, T.; et al.. **Single-phase ferritic solidification mode in austenitic-ferritic stainless steel welds.**Metallurgical Transactions A, vol. 10A, p. 1183-1190, 1979.

[23] JOHNSON, E.; GRABAEK, L.; et al. **Microstructure of rapidly solidified stainless steel.** Materials Science and Engineering, vol. 98, p. 301-303, 1988.

[24] HAMMAR, O.; SVENSSON, U.. **Influence of Steel Composition on Segregation and Microstructure During Solidification of Austenitic Stainless Steels.** Solidification and Casting Metals, London, Metals Society, p. 401- 410, 1979.

[25] ASTM E1086-08: Standard Test Method for Optical Emission Vacuum Spectrometric Analysis of Stainless Steel by the Point-to-Plane Excitation Technique. ASTM International. West Conshohocken. PA. EUA. 2008.

[26] ASTM E562-08: Standard Test Method for Determining Volume Fraction by Systematic Manual Point Count. ASTM International. West Conshohocken. PA. EUA. 2008.